

Combining Molecular Dynamics with Lattice–Boltzmann: A Hybrid Method for the Simulation of (Charged) Colloidal Systems

Apratim Chatterji and Jürgen Horbach*

Institut für Physik, Johannes Gutenberg–Universität Mainz, D–55099 Mainz, Germany

Abstract

We present a hybrid method for the simulation of colloidal systems, that combines molecular dynamics (MD) with the Lattice–Boltzmann (LB) scheme. The LB method is used as a model for the solvent in order to take into account the hydrodynamic mass and momentum transport through the solvent. The colloidal particles are propagated via MD and they are coupled to the LB fluid by viscous forces. With respect to the LB fluid, the colloids are represented by uniformly distributed points on a sphere. Each such point (with a velocity $\mathbf{V}(\mathbf{r})$ at any off–lattice position \mathbf{r}) is interacting with the neighboring eight LB nodes by a frictional force $\mathbf{F} = \xi_0(\mathbf{V}(\mathbf{r}) - \mathbf{u}(\mathbf{r}))$ with ξ_0 being a friction force and $\mathbf{u}(\mathbf{r})$ being the velocity of the fluid at the position \mathbf{r} . Thermal fluctuations are introduced in the framework of fluctuating hydrodynamics. This coupling scheme has been proposed recently for polymer systems by Ahlrichs and Dünweg [J. Chem. Phys. **111**, 8225 (1999)]. We investigate several properties of a single colloidal particle in a LB fluid, namely the effective Stokes friction and long time tails in the autocorrelation functions for the translational and rotational velocity. Moreover, a charged colloidal system is considered consisting of a macroion, counterions and coions that are coupled to a LB fluid. We study the behavior of the ions in a constant electric field. In particular, an estimate of the effective charge of the macroion is yielded from the number of counterions that move with the macroion in the direction of the electric field.

PACS numbers: 47.65.+a, 82.70.Dd, 47.11.+j, 83.85.Pt, 05.20.Dd, 07.05.Tp, 66.20.+d

I. INTRODUCTION

In colloidal suspensions, big molecules (colloids) with a typical size of the order of 10 nm to several μm are immersed in an atomistic solvent^{1,2}. A detailed modeling of such systems would be provided by a molecular dynamics (MD) simulation where both colloids and solvent atoms are propagated via Newton's equations of motion. However, this approach has severe drawbacks due to the large size difference between colloids and solvent particles. One would have to take into account the microscopic details of a large amount of solvent particles which are irrelevant on the typical length and time scale of the colloids. In order to circumvent this problem, one may describe the interactions between the colloids by an effective potential, thus avoiding the explicit consideration of the solvent's degrees of freedom². But then the hydrodynamic mass and momentum transport through the solvent is completely neglected and hence, hydrodynamic interactions between colloidal particles are not taken into account. But it is well-known that many transport properties in colloidal suspensions are affected by hydrodynamic interactions^{1,2}.

In recent years many efforts have been undertaken to model colloidal suspensions by mesoscopic simulation techniques. The idea is to describe the solvent on a coarse-grained level, whereby the properties of the solvent on hydrodynamic time and length scales are correctly recovered. Different approaches exist in the literature that range from particle-based methods such as dissipative particle dynamics (DPD)^{3,4,5,6} and stochastic rotation dynamics (SRD)^{7,8,9,10,11} to the Lattice-Boltzmann (LB) method^{12,13,14} where the Navier-Stokes equations are solved on a lattice via a kinetic equation. All these methods have their advantages and disadvantages, and they might provide complementary information for a given problem.

In this paper, we present a hybrid MD/LB method for the simulation of colloidal systems. In this approach, the coupling between colloids and solvent (LB fluid) is realized locally at the surface of the colloids. The modeling of the solvent by a LB fluid has the advantage that hydrodynamic properties of the solvent (e.g., the shear viscosity η) are incorporated as input parameters, and thus they can be varied over a broad range (compared to particle-based methods). Moreover, the LB method allows to implement easily the rotational degrees of freedom of the colloids, an issue that is difficult to handle in particle-based models of the solvent.

Several methods have been proposed for the introduction of colloidal particles in a LB fluid. In Ladd’s method^{12,13,15}, a colloid is represented by its surface which cuts some of the links between lattice nodes of the LB fluid. Halfway along these links, boundary points are placed where the one-particle distribution functions, that represent fluid populations, are bounced back such that no-slip boundary conditions are obtained. A different approach for the particle–fluid coupling has been proposed by Lobaskin *et al.*¹⁶ Here, a colloid is represented by point particles that are connected with each other by springs (modeled by a FENE potential). The latter point particles interact with the fluid locally via a friction force^{17,18,19}. The coupling scheme that we present in this paper can be seen as one in between Ladd’s bounce back rules and the frictional coupling scheme of Lobaskin *et al.* As in Ladd’s method, each colloid is represented by boundary points on its surface and the total force and torque that is exerted on a colloid by the fluid is obtained by summing up all the contributions from the boundary points. Different from Ladd’s method we use local friction forces between the boundary points and the fluid as proposed by Lobaskin *et al.* However, no interaction potential between boundary points is required in our scheme. We also avoid some inherent problems of Ladd’s method. Our scheme does not introduce shape fluctuations of a moving colloidal particle as well as mass fluctuations in the fluid that are induced by the bounce back rules on a moving colloidal particle.

Many attempts have been devoted very recently to the development of simulation methods for charged colloids, using the LB method or finite difference schemes to model hydrodynamic interactions. These approaches consider charged colloids in the framework of the primitive model², i.e. as a system of negatively charged macroions, small counterions of positive charge and small coions of negative charge. In Refs.^{20,21,22,23} the small ions are modeled as charge densities on the level of the Poisson–Boltzmann equation. The propagation of these charge densities is achieved by the so-called electrokinetic equations¹ that couple the Navier–Stokes equations with a dynamic generalization of the Poisson–Boltzmann equation. The description of charged colloids by the electrokinetic equations has some drawbacks: Of course, correlations between the ions are neglected, since the Poisson–Boltzmann equation is a mean-field description. Moreover, it is not clear how one can properly introduce thermal fluctuation in the electrokinetic equations and thus, so far only calculations at zero temperature are possible. Therefore, Lobaskin *et al.*²⁴ have followed a different strategy by considering explicitly small ions that are moved together with macroions by their hybrid

MD/LB scheme. Using MD/LB approach, we also model charged colloidal systems in this way, and, as an application we consider below the problem of a charged colloidal system in an external electric field.

The rest of the paper is organized as follows: In the next section, we give a brief introduction to the LB method. Then, we present our scheme to couple colloidal particles with a LB fluid (Sec. III) and the use of this scheme in a hybrid MD/LB method (Sec. IV). Applications are shown in Sec. V where a neutral colloid in a LB fluid is considered as well as a macroion and small ions in a LB fluid that are subject to an external electric field. Finally, we summarize and discuss the method and the results.

II. LATTICE BOLTZMANN METHOD

In this section, we briefly describe the LB method used in our work. A detailed description can be found in several review articles^{12,13} and in the book by Succi¹⁴.

In the LB method a discretized version of a simple kinetic equation is solved numerically on a lattice. The central quantity in this equation is an one-particle distribution function $n_i(\mathbf{r}, t)$ which gives the particle population on a lattice node \mathbf{r} at time t with a discrete velocity \mathbf{c}_i . The discrete space of velocities $\{\mathbf{c}_i\}$ has to be constructed such that the underlying kinetic equation is consistent with the Navier–Stokes equations. In particular, the $\{\mathbf{c}_i\}$ should not introduce any artificial anisotropies in the hydrodynamic equations. Several choices for $\{\mathbf{c}_i\}$ are possible. In this work, the velocity space consists of 18 vectors placed on lattice nodes of a cubic lattice, 6 of these point to the nearest neighboring nodes and 12 to the next-nearest neighboring nodes. These velocity vectors have the absolute values $1 a/\tau$ and $\sqrt{2} a/\tau$, respectively, with a being the lattice spacing and τ the elementary time unit. Note that the latter velocity space can be constructed by projecting the 24 unit vectors of a four dimensional FCHC lattice onto three dimensions.

The equations of motion for the $n_i(\mathbf{r}, t)$ can be written as

$$n_i(\mathbf{r} + \mathbf{c}_i\tau, t + \tau) = n_i(\mathbf{r}, t) + \Delta_i[\{n_i(\mathbf{r}, t)\}], \quad (1)$$

where the collision operator Δ_i describes the change of n_i due to collisions between the particles (of course Δ_i has to be further specified). The moments of $n_i(\mathbf{r}, t)$ are hydrodynamic

fields, namely the mass density

$$\rho(\mathbf{r}, t) = \sum_{i=1}^{18} n_i(\mathbf{r}, t) , \quad (2)$$

the momentum density

$$\mathbf{j}(\mathbf{r}, t) = \sum_{i=1}^{18} n_i(\mathbf{r}, t) \mathbf{c}_i , \quad (3)$$

and the momentum flux

$$\mathbf{\Pi}(\mathbf{r}, t) = \sum_{i=1}^{18} n_i(\mathbf{r}, t) \mathbf{c}_i \mathbf{c}_i . \quad (4)$$

Note that \mathbf{j} can be also written as $\mathbf{j} \equiv \rho \mathbf{u}$ with \mathbf{u} denoting the flow velocity.

The aim is to construct the collision operator Δ_i in as simple a form as possible such that the time evolution for the moments in Eqs. (1)–(4) is consistent with the Navier–Stokes equations. To this end, we assume that Δ_i describes small deviations from equilibrium. Hence, it can be given in a linearized form,

$$\Delta_i[\{n_i(\mathbf{r}, t)\}] = \sum_{j=1}^{18} L_{ij} (n_j(\mathbf{r}, t) - n_j^{\text{eq}}) , \quad (5)$$

where n_i^{eq} is the local equilibrium distribution function and L_{ij} denotes a matrix element of the collision operator.

The equilibrium population n_i^{eq} can be expressed as^{12,14}

$$n_i^{\text{eq}} = a^{c_i} \left[\rho + \frac{1}{c_s^2} \rho \mathbf{u} \cdot \mathbf{c}_i + \frac{1}{c_s^4} \rho \mathbf{u} \mathbf{u} : (\mathbf{c}_i \mathbf{c}_i - c_s^2 \mathbf{1}) \right] , \quad (6)$$

where n_i^{eq} depends only on ρ and \mathbf{u} . The parameter c_s in Eq. (6) denotes the sound velocity. The values for c_s as well as for the coefficients a^{c_i} can be fixed by a Chapman–Enskog expansion such that the Navier–Stokes equations in the limit of small \mathbf{u} are recovered. This yields $c_s = \sqrt{1/2}$. The parameters a^{c_i} can have the two values a^1 and $a^{\sqrt{2}}$ where the superscript corresponds to the absolute value of the velocity vector. In our case, we have $a^1 = 1/12$ and $a^{\sqrt{2}} = 1/24$. The conservation of mass and momentum requires that ρ and \mathbf{j} are unaffected by the collision operator. The kinematic viscosity ν is related to the eigenvalue λ of L_{ij} that corresponds to the eigenvector $c_{i\alpha} c_{j\beta}$ (herein, the indices α, β with $\alpha \neq \beta$ denote the Cartesian components):

$$\nu = -\frac{1}{6} \left(\frac{2}{\lambda} + 1 \right) \frac{a^2}{\tau} \quad (7)$$

In the following we choose $\lambda = -1.75$ which corresponds to $\nu = 0.0238 a^2/\tau$.

All non-hydrodynamic modes (ghost modes), that are due to the use of a lattice, are suppressed by setting the corresponding eigenvalues of L_{ij} to -1. Since we are interested in incompressible LB fluids also the eigenvalue related to the bulk viscosity is chosen to be -1.

As shown by Ladd²⁶, the LB scheme as defined by Eqs. (1)–(7) allows also the introduction of thermal fluctuations. This can be done in the framework of fluctuating hydrodynamics²⁷. To this end, one adds an additional stochastic term n'_i in Eq. (1) which represents the addition of thermal fluctuations to the stress tensor,

$$n'_i = -\frac{a^{c_i}}{c_s^4} \sum_{\alpha\beta} \sigma'_{\alpha\beta} c_{i\alpha} c_{i\beta} . \quad (8)$$

The random stresses $\sigma'_{\alpha\beta}$ are random numbers with zero mean and white noise behavior, i.e.

$$\begin{aligned} & \langle \sigma'_{\alpha\beta}(\mathbf{r}, t) \sigma'_{\gamma\delta}(\mathbf{r}', t') \rangle \\ &= A \delta_{\mathbf{r}\mathbf{r}'} \delta_{tt'} \left(\delta_{\alpha\gamma} \delta_{\beta\delta} + \delta_{\alpha\delta} \delta_{\beta\gamma} - \frac{2}{3} \delta_{\alpha\beta} \delta_{\gamma\delta} \right) \end{aligned} \quad (9)$$

where the δ 's are Kronecker deltas and A is a constant which has to be chosen such that the fluctuation-dissipation theorem holds. The latter condition requires the choice $A = 2\eta k_B T \lambda^2$.

An elementary step in a LB simulation can be decomposed in a collision step and a propagation step. In the collision step, the interaction between the “particles” at node \mathbf{r} at the collision time t^* is taken into account that results in the postcollision function

$$n_i^*(\mathbf{r}, t^*) = n_i(\mathbf{r}, t^*) + \Delta_i[\{n_i\}] + n'_i(\mathbf{r}, t^*). \quad (10)$$

Using the $n_i^*(\mathbf{r}, t^*)$, the n_i can be updated in the propagation step,

$$n_i(\mathbf{r} + \mathbf{c}_i, t + 1) = n_i^*(\mathbf{r}, t^*) . \quad (11)$$

In our implementation we have omitted non-linear terms in \mathbf{u} and thus, we describe a fluid on the level of the linearized Navier-Stokes equations (for more details see Refs.^{12,13}).

III. THE COUPLING OF THE LB FLUID TO COLLOIDAL PARTICLES

Consider a Brownian particle of mass M in a solvent. In first approximation, one can describe the motion of the particle without taking into account explicitly the solvent particles. To this end, one assumes that, on the typical Brownian time scale, the collisions of

the particle with the solvent particles can be modeled by Gaussian random forces \mathbf{f}_r . These forces lead to a systematic friction force $-\xi_0\mathbf{V}(t)$ on the particle where ξ_0 is the friction coefficient and $\mathbf{V}(t)$ the velocity of the particle at time t . The resulting equation of motion is a Langevin equation (see, e.g., Ref.¹),

$$M\frac{d^2\mathbf{r}}{dt^2} = \mathbf{F}_c - \xi_0\mathbf{V}(t) + \mathbf{f}_r . \quad (12)$$

Here, \mathbf{r} is the position of the particle and \mathbf{F}_c denotes a conservative force due to the interaction with other particles. The Cartesian components of the forces, $f_{r,\alpha}$, are random numbers that are uncorrelated with zero mean, i.e.

$$\langle f_{r,\alpha}(\mathbf{r}, t) \rangle = 0 \quad (13)$$

$$\langle f_{r,\alpha}(\mathbf{r}, t) f_{r,\beta}(\mathbf{r}', t') \rangle = A\delta_{\alpha\beta}\delta(\mathbf{r} - \mathbf{r}')\delta(t - t') . \quad (14)$$

The amplitude A is given by the fluctuation–dissipation theorem, $A = 2k_B T \xi_0$.

In Eq. (12) the interaction of the Brownian particle with the solvent is described by the force $\mathbf{F}_B = -\xi_0\mathbf{V}(t) + \mathbf{f}_r$. By this force, transport of momentum in the fluid due to the motion of the particle is not taken into account and thus one does not recover the correct hydrodynamic behavior of the Brownian particle. This is reflected, e.g., in the behavior of the velocity autocorrelation function $C_v(t)$. For a single particle, propagated according to Eq. (12) (with $\mathbf{F}_c = 0$), $C_v(t)$ decays exponentially, $C_v(t) \propto \exp(-\xi_0 t/M)$, whereas the correct hydrodynamic behavior is a power law decay at long times, $C_v(t) \propto t^{-3/2}$ (the so-called long-time tail)¹. However, in order to incorporate hydrodynamics, Eq. (12) can be easily modified by coupling the Brownian particle to a LB fluid. The essential point is to replace the *absolute* velocity $\mathbf{V}(t)$ of the particle in the frictional force term by its velocity relative to the fluid. The force \mathbf{F}_B is then modified to

$$\mathbf{F}_B = -\xi_0 (\mathbf{V}(\mathbf{r}, t) - \mathbf{u}(\mathbf{r}, t)) + \mathbf{f}_r \quad (15)$$

where $\mathbf{u}(\mathbf{r}, t)$ is the velocity of the fluid at the position of the particle. Since the position of the particle is continuous in space, we have to use an interpolation scheme to determine $\mathbf{u}(\mathbf{r}, t)$. As in Ref.^{18,19}, we use a linear interpolation scheme that estimates $\mathbf{u}(\mathbf{r}, t)$ from the eight nearest lattice nodes around \mathbf{r} . Of course, Newton’s third law requires that whenever the Brownian particle is subject to a force \mathbf{F}_B as given by Eq. (15), the force $-\mathbf{F}_B$ has to be applied to the fluid nodes with which the particle interacts (see Refs.^{18,19}). One may

wonder why fluctuations have to be added both to the LB fluid and the Brownian particle. However, it was shown in Ref.²⁵ that only then the fluctuation–dissipation theorem holds for the total system of a particle in a LB fluid coupled via Eq. (15).

Up to now we have considered the Brownian particle as a point particle which has, in particular, no rotational degrees of freedom (however, its effective hydrodynamic radius with respect to the LB fluid is of the order of the lattice spacing a). In order to model an extended object, such as a sphere of radius R , the force coupling as given by Eq. (15) can be generalized as follows: As in Ladd’s method^{12,13} the sphere is represented by boundary points on its surface, whereby the surface is permeable for the LB fluid. In our method, the boundary points are placed uniformly on the surface of the sphere. The uniform distribution of boundary points can be achieved by the following iterations: One starts from points that are placed at the corners of an octahedron. The envelope of this octahedron is a sphere of radius R , the centre of which is denoted by \mathbf{R}_{cm} in the following. Then one places new points halfway along the twelve edges of the octahedron and shifts these points such that they sit on the surface of the latter sphere. As a result, a polygon with 18 corners and 48 edges is obtained. In this object, again new points are placed halfway along the edges and shifted to the surface of the enveloping sphere. This object has now 66 corners, i.e. 66 boundary points, and is used in this work as a model for a colloidal particle. A snapshot is shown in Fig. 1. We consider that each of the boundary nodes has a mass $M/66$ where M is the mass of the colloidal particle. Each of the boundary points is coupled to the LB fluid according to Eq. (15). The total force on the particle is then determined by the sum

$$\mathbf{F}_{\text{B,tot}} = \sum_{i_{\text{b}}=1}^{66} \mathbf{F}_{\text{B}}(\mathbf{r}_{i_{\text{b}}}) \quad (16)$$

where $\mathbf{r}_{i_{\text{b}}}$ denotes the positions of the 66 boundary points. The torque that is exerted on the particle by the fluid is updated via

$$\mathbf{T}_{\text{B}} = \sum_{i_{\text{b}}=1}^{66} \mathbf{F}_{\text{B}}(\mathbf{r}_{i_{\text{b}}}) \times (\mathbf{r}_{i_{\text{b}}} - \mathbf{R}_{\text{cm}}) . \quad (17)$$

$\mathbf{F}_{\text{B,tot}}$ and \mathbf{T}_{B} can be used to update the translational and the rotational velocity of the colloidal particle which we denote by \mathbf{V}_0 and ω_0 , respectively. The simplest discretized form of the equations of motion is the Euler algorithm which is of first order in the time step h

for the integration,

$$\mathbf{V}_0(t+h) = \mathbf{V}_0(t) + \mathbf{F}_{\text{B,tot}} \frac{h}{M} \quad (18)$$

$$\omega(t+h) = \omega(t) + \mathbf{T}_B \frac{h}{I}. \quad (19)$$

In Eq. (19), I is the moment of inertia of the particle. The Euler algorithm has of course very bad properties with respect to stability, temperature drift etc. In the next section, we present an integrator based on the Heun algorithm²⁸ that is of second order in h .

The boundary points that we use for the representation of the surface of the spherical particle are not rotated according to the updated rotational velocity ω_0 . These points are fixed with respect to the centre of mass position \mathbf{R}_{cm} of the particle. The idea is that the surface of a spherical particle can be always represented by the same set of uniformly distributed points if the surface grid that they form is fine enough. We have checked that the sphere with 66 boundary points (see Fig. 1) is sufficient for particle radii up to $R = 5.0a$. In this case, no change in any physical properties is seen if the particle is decorated with more boundary points.

IV. THE HYBRID MD/LB SCHEME

Now, we discuss the algorithm that we use for the integration of the equations of motion of a system of colloidal particles coupled to a LB fluid. To this end, we use a generalized velocity Verlet algorithm²⁹. For the colloidal particles we use the model with 66 boundary points that we have described in the previous section.

The force on particle i can be decomposed into three terms,

$$\mathbf{F}_{\text{tot},i} = \mathbf{F}_{\text{c},i} + \mathbf{F}_{\text{f},i} + \mathbf{F}_{\text{r},i}, \quad (20)$$

where $\mathbf{F}_{\text{c},i}$ is the contribution from conservative forces. $\mathbf{F}_{\text{f},i}$ and $\mathbf{F}_{\text{r},i}$ denote friction and random forces, respectively. To compute $\mathbf{F}_{\text{f},i}$, one sums up the contributions from the 66 boundary points,

$$\mathbf{F}_{\text{f},i} = - \sum_{i_b=1}^{66} \xi_{0,i_b} [\mathbf{v}_i + \omega \times (\mathbf{r}_{i_b} - \mathbf{r}_i) - \mathbf{u}(\mathbf{r}_{i_b})], \quad (21)$$

where \mathbf{r}_i and \mathbf{v}_i are respectively the position and the velocity of the centre of mass of particle i , \mathbf{r}_{i_b} is the position of the boundary node i_b of particle i , ω is its angular velocity, and the

fluid velocities at the boundary points are denoted by $\mathbf{u}(\mathbf{r}_{i_b})$. ξ_{0,i_b} is the friction coefficient of boundary point i_b and thus the total friction coefficient ξ_0 is given by $\xi_0 = \sum_{i_b} \xi_{0,i_b}$. In the following, each of the 66 ξ_{0,i_b} is assigned the same value $\xi_0/66$ for a given particle.

The random force can be written as

$$\mathbf{F}_{r,i} = \sqrt{2\pi k_B T} \sum_{i_b=1}^{66} \sqrt{\xi_{0,i_b}} \theta_{i_b}. \quad (22)$$

Here, the θ_i is a vector of random numbers with the Cartesian components $\theta_{i,\alpha}$ ($\alpha \in \{x, y, z\}$) for which

$$\langle \theta_{i,\alpha}(t) \rangle = 0 \quad (23)$$

$$\langle \theta_{i,\alpha}(t) \theta_{j,\beta}(t') \rangle = \delta_{ij} \delta_{\alpha\beta} \delta(t - t') \quad (24)$$

holds. Note that it is not necessary to use random numbers $\theta_{i,\alpha}$ with a Gaussian distribution for the numerical integration. It was shown in Ref.³⁰ that it is sufficient to use uniform random numbers that fulfill the requirements as given by Eqs. (23) and (24).

The update of the centre of mass positions of the particles is similar to that in the velocity Verlet algorithm²⁹. In an integration time step h the position change from $\mathbf{r}_i(0)$ to

$$\begin{aligned} \mathbf{r}_i(h) &= \mathbf{r}_i(0) + h\mathbf{v}_i(0) \\ &\quad + \frac{h^2}{2M} (\mathbf{F}_{c,i}(0) + \mathbf{F}_{f,i}(0)) + \mathbf{F}_{r,i}(h). \end{aligned} \quad (25)$$

For the determination of the velocities $\mathbf{v}_i(h)$, the friction force $\mathbf{F}_{f,i}$ at time $t = h$ is needed if we want to apply the velocity Verlet scheme. But in this case, the problem arises that $\mathbf{F}_{f,i}(h)$ depends itself on $\mathbf{v}_i(h)$. This problem can be solved if we first approximate $\mathbf{v}_i(h)$ in an Euler step to obtain

$$\mathbf{v}_i^*(h) = \mathbf{v}_i(0) + \frac{h}{M} (\mathbf{F}_{c,i}(0) + \mathbf{F}_{f,i}(0)) + \frac{h}{M} \mathbf{F}_{r,i}(h), \quad (26)$$

where the star indicates that we use this velocity only for an estimate of $\mathbf{F}_{f,i}(h)$. Also the angular velocity $\omega_i(h)$ is updated by an Euler step,

$$\omega_i(h) = \omega_i(0) + \frac{h}{I} \sum_{i_b=1}^{66} \mathbf{F}_f(0) \times [\mathbf{r}_{i_b} - \mathbf{r}_i(h)]. \quad (27)$$

With Eqs. (26) and (27) we yield the friction force at time $t = h$ as

$$\begin{aligned} \mathbf{F}_{f,i}(h) &= - \sum_{i_b=1}^{66} \xi_{0,i_b} [\mathbf{v}_i^*(h) + \omega(h) \times (\mathbf{r}_{i_b} - \mathbf{r}_i(h)) \\ &\quad - \mathbf{u}(\mathbf{r}_{i_b})]. \end{aligned} \quad (28)$$

With Eq. (28) the velocities $\mathbf{v}_i(h)$ are obtained by

$$\begin{aligned} \mathbf{v}_i(h) = & \mathbf{v}_i(0) + \frac{h}{2m} [\mathbf{F}_{c,i}(0) + \mathbf{F}_{c,i}(h) \\ & + \mathbf{F}_{f,i}(0) + \mathbf{F}_{f,i}(h) + 2\mathbf{F}_{r,i}(h)] \end{aligned} \quad (29)$$

Of course, at the same time one has to transfer also the force $-\mathbf{F}_{f,i}(h) - \mathbf{F}_{r,i}(h)$ to the appropriate nodes in the LB fluid.

Our scheme is equivalent to the Heun algorithm²⁸ which is a standard method for the solution of Langevin equations^{31,32}. If we set $\xi_{0,i_b} = 0$ in Eqs. (25) and (29) the algorithm reduces to the velocity Verlet algorithm for the microcanonical ensemble²⁹.

V. RESULTS

In this section we present several applications of our MD/LB method. First, we consider a neutral colloidal particle in a LB fluid to calculate its effective friction coefficient (part A) and to study long time tails in the translational and rotational velocity autocorrelation function (part B). In part C we consider a charged colloid in an electric field. In the following, we choose $\rho = 1.0 m_0/a^3$ for the density and $\eta \equiv \nu\rho = 0.02381a^2\rho/\tau$ for the shear viscosity of the LB fluid.

A. Friction coefficient

Consider a sphere with (hydrodynamic) radius R_h that moves through a viscous fluid due to a gravitational field \mathbf{g} . In the steady state, it experiences a drag force \mathbf{F}_d which is proportional to its velocity \mathbf{U} , according to Stokes law³³:

$$\mathbf{F}_d = \xi\mathbf{U} \quad (30)$$

where ξ is the Stokes friction coefficient. In the case of no-slip boundary conditions, the friction coefficient is given by $\xi = 6\pi\eta R_h$ (with η being the shear viscosity of the fluid). In the steady state, the force \mathbf{F}_d is equal to the gravitational force on the sphere,

$$\mathbf{F}_g = \frac{4}{3}\pi R_h^3(\rho_p - \rho)\mathbf{g}, \quad (31)$$

where ρ_p and ρ denote the density of the sphere and the fluid, respectively. Thus, from $\mathbf{F}_g = \mathbf{F}_d$ the friction coefficient ξ can be determined by measuring the velocity \mathbf{U} of the particle in the steady state.

As a convenient way to determine ξ in a LB simulation, we follow here the scheme proposed by Ladd¹². We consider a particle in a LB fluid. This system is put in a cubic box of volume $V = L^3$ with periodic boundary conditions in all three Cartesian directions x, y, z . The particle is held fixed by assigning an infinite mass to it. Then, a pressure gradient $\nabla_x p$ is introduced in the x direction by applying a constant increment Δj_x to the x component of the momentum density at each lattice node. In the steady state, the total force on the particle is balanced by the sum of the drag force $F_{d,x} = V\Delta j_x/\tau$ and the buoyancy force $F_b = -\frac{4}{3}\pi R^3\Delta j_x/\tau$ (remember that τ denotes the time step of the LB simulation). Thus the Stokes friction coefficient is given by $\xi_L = F_{d,x}/U_x$ where the index L reflects that the particle is moving in a finite system of size L . Due to the periodic boundary conditions, ξ_L describes the friction of an array of spheres that sit on a cubic lattice with lattice constant L . An analytic expression for $1/\xi_L$ in terms of an expansion of powers of $1/L$ was first derived by Hasimoto³⁴ assuming no-slip boundary conditions. It has the following form:

$$\frac{1}{\xi_L} = \frac{1}{6\pi\eta} \left(\frac{1}{R_h} - \frac{2.837}{L} + \frac{4.19}{L^3} R_h^2 + \dots \right) \quad (32)$$

For our fluid-particle coupling scheme, we can only use this formula for high values of ξ_0 . Then, no-slip boundary conditions are approximately recovered as we shall see in the following.

In Fig. 2, $1/\xi_L$ is plotted as a function of $1/L$ for different values of ξ_0 from $\xi_0 = 3.3 m_0/\tau$ to $\xi_0 = 19.8 m_0/\tau$. The radius of the particle is $R = 2.5a$ in this case. For $1/L < 0.04a^{-1}$ the data can be well described by a linear $1/L$ dependence of the form

$$\frac{1}{\xi_L} = \frac{1}{\xi_\infty} - B\frac{1}{L}, \quad (33)$$

where ξ_∞ denotes the friction coefficient for an unbounded system. Fits with Eq. (33) are shown in Fig. 2 as dashed lines. In these fits, the slope B changes only slightly with ξ_0 : We find $B = 6.419a\tau/m_0$ at $\xi_0 = 3.3 m_0/\tau$ and $B = 6.438a\tau/m_0$ at $\xi_0 = 19.8 m_0/\tau$. Moreover, for $\xi_0 = 19.8 m_0/\tau$ the data over the full $1/L$ range can be well described by a fit with Eq. (32) (bold solid line in Fig. 2). In the latter fit only the hydrodynamic radius R_h was used as a fit parameter for which we find $R_h = 3.05a$. The good quality of the fit indicates that at $\xi_0 = 19.8 m_0/\tau$, no-slip boundary conditions are almost recovered whereas at smaller values of ξ_0 mixed stick-slip boundary conditions are obtained. This can be also inferred from the inset of Fig. 2 where we have plotted R_h/R as determined from the fitted ξ_∞ via $R_h/R = \xi_\infty/(6\pi\eta R)$.

One may wonder why the hydrodynamic radius is about 20% higher than the assigned radius $R = 2.5a$ of the particle. But this is just an artifact of the discrete nature of the LB fluid. This artifact can be reduced by increasing the size of the particle.

The discrete nature of the LB fluid is also reflected in the dependence of ξ on the size of the particle R . In Fig. 3, we show ξ as a function of R for the two system sizes $L = 60a$ and $L = 80a$. We see from the figure that, at small values of R , ξ_L does not increase linearly with the sphere radius R and thus the ratio R_h/R is not a constant in this regime. Only, for $R > 3.0a$, $\xi_L \propto R$ seems to hold to a good approximation.

We have seen that, with the frictional coupling scheme used in this work, no-slip boundary conditions at the surface of a colloidal particle can be nearly realized. For the system considered in this section, one has to choose a value of ξ_0 around $20 m_0/\tau$ to obtain no-slip boundary conditions. Note that the limit of small values of ξ_0 is also of interest. As we shall demonstrate in a forthcoming publication³⁵, the frictional coupling scheme can be also used to model walls at which mixed stick-slip boundary conditions hold. This is an important issue for the modeling of fluids in nanoscopic slits.

B. Long time tails

In this section, we consider again a neutral, spherical particle in a LB fluid. Our aim is to study the normalized translational and rotational velocity autocorrelation function which we denote by $C_v(t)$ and $C_\omega(t)$, respectively. These functions can be simply calculated by making use of linear response theory. To this end, we consider a colloidal particle in a LB fluid at rest. At $t = 0$, we give the particle a translational or rotational velocity. The decay of these velocities with time, normalized by the initial values, yields then the functions $C_v(t)$ and $C_\omega(t)$, respectively.

Fig. 4 illustrates the short time decay of $C_v(t)$ for different values of ξ_0 . The initial decay of these functions is given by the exponential functions $f(t) = \exp(-\frac{\xi_0}{M}t)$ which are shown as dotted lines in Fig. 4 (note that we have assigned the mass $M = 120m_0$ to the particle). Thus, the short time behavior of $C_v(t)$ is completely controlled by the relaxation time $\tau_B = M/\xi_0$.

As we can also see in Fig. 4, for $t > \tau_B$ the the average fluid velocity at the surface of the particle essentially equals the velocity of the particle. The dashed lines in Fig. 4 are

averaged velocities v_s of the fluid at the boundary points of the particle (normalized by the initial velocity $V(0)$ of the particle). Obviously, $v_s/V(0)$ matches the function $C_v(t)$ at a time which is of the order of τ_B .

For long times one expects the occurrence of a long time tail in $C_v(t)$, i.e., a decay with the power law $f(t) = At^{-3/236}$. The theoretical prediction for the prefactor is $A = M/(12\rho)[\pi\nu]^{-3/237,38}$ (with $\nu = \eta/\rho$ being the kinematic viscosity of the fluid). According to this prediction the prefactor A does not depend on the details of the particle such as its radius R . The physical origin of the long time tail is the conservation of momentum, which is transported away diffusively from the particle. Since the momentum transport in a fluid is spatially long-ranged, one expects the presence of finite size effects if the decay of velocity correlations of a colloidal particle in a finite simulation box is considered.

In Fig. 5, $C_v(t)$ is plotted for different system sizes L for $\xi_0 = 6.6 m_0/\tau$ and, as a dotted line, the theoretically predicted long time tail is shown (note that no fit parameters are involved). We see that the theoretical result match perfectly with the simulation data. One can also infer from the figure the expected finite size effects. At a given L , C_v seems to approach a constant at long enough times. This is just a consequence of momentum conservation: At long times the particle has completely transferred its initial velocity v_0 to the LB fluid and then the whole system moves with a constant velocity v_0/N_{tot} where N_{tot} is the total number of lattice nodes.

Also the angular velocity correlation function $C_\omega(t)$ exhibits a long time tail but now the exponent for the power law decay is $-5/2$, i.e. $f(t) = Bt^{-5/2}$. The theoretical prediction for the prefactor is $B = \pi I/\rho [4\pi\nu]^{-5/239}$. In order to compare the latter theoretical prediction to the simulation result, one has to estimate the moment of inertia I of the rotating sphere. On the one hand, I has a contribution I_1 from the shell of the particle that consists of 66 boundary points. On the other hand, at long times the moment of inertia is also affected by the rotating fluid inside the sphere which leads to a second contribution I_2 to I . I_1 can be estimated by $I_1 = \frac{2}{3}MR^2 = 500 m_0a^2$ (i.e., the value of a hollow sphere with radius R). We have computed I_2 numerically by considering all the lattice nodes of mass m_0 inside the sphere to obtain the value $I_2 = 228 m_0a^2$. Thus, the total moment of inertia of the rotating sphere is $I = I_1 + I_2 = 728 m_0a^2$. The theoretical prediction using this value of I is shown in Fig. 6 in comparison with the simulation data for different values of L . Obviously, the theoretical prediction is in nice agreement with the numerical data.

As we have already mentioned, we use linear response theory to determine $C_v(t)$ and $C_\omega(t)$ by considering a kicked particle in a LB fluid which is initially at rest. Of course, we can also calculate the velocity correlation functions from thermal fluctuations of the translational and rotational velocity, respectively, and this should yield identical results. Indeed, this is the case as we can infer from Fig. 7 and Fig. 8 where $C_v(t)$ and $C_\omega(t)$, respectively, are shown for $L = 40a$ and $\xi_0 = 6.6 m_0/\tau$.

We have seen in this section that we recover the theoretical predictions for the long time tails in $C_v(t)$ and $C_\omega(t)$. This is in agreement with the study of Lobaskin *et al.*¹⁶ who use a slightly different particle–fluid coupling scheme (see above).

C. Charged Colloids

Now we demonstrate that our hybrid MD/LB scheme can be applied to charged colloidal systems. To this end, we consider a charged spherical particle (macroion) that is immersed in a fluid of small ions and a neutral “hydrodynamic background” which is modeled by a LB fluid. This system is then studied in an electric field to determine the drift velocity and the effective dynamic charge of the macroion. In the following, we first introduce the model and the simulation details, before we present the results of the simulation.

1. Model and simulation details

A potential that describes surprisingly well the effective interactions between macroions in a charged colloidal suspension is the Debye–Hückel (DH) potential, which is the solution of the linearized Poisson–Boltzmann equation¹. This potential has a Yukawa form,

$$u(r) = K \frac{\exp(-r/\lambda_D)}{r}, \quad (34)$$

where λ_D is the so-called Debye screening length and K is a constant depending in particular on the charge of the macroions Z_m . Eq. (34) describes the screening of the Coulomb interaction between positively charged macroions due to the presence of small ions in the system, namely negatively charged counterions and positively charged coions. The screening length is explicitly given by $\lambda_D = (4\pi l_B \sum_s z_s^2 \bar{\rho}_s)^{-1/2}$ where l_B is the Bjerrum length and $\bar{\rho}_s$ is the average density of microscopic ions of type s (either counterions or coions). In

principal the DH potential should only be valid for small charge and surface potential of the macroions. However, it turns out that also systems with highly charged particles can be rather well described by the DH potential if one introduces an effective charge Z_m^* for the macroions. One possibility to determine Z_m^* experimentally is via electrophoresis where the Z_m^* is extracted from the measurement of the electrophoretic mobility (see below). We shall address here the problem of estimating Z_m^* via electrophoresis by means of our LB/MD simulation method.

To this end, we investigate a charged colloidal system in the framework of the primitive model¹. Thus, we consider a system of a positively charged macroion of charge Z_m and small ions of charge $Z_i = -1$ (counterions) and of charge $Z_c = 1$ (coions). Of course, the number of counterions and coions is chosen such that charge neutrality of the system holds. The interaction potential between a particle of type α and a particle of type β ($\alpha, \beta = m, i, c$) separated by a distance r from each other is given by

$$u_{\alpha\beta} = \frac{Z_\alpha Z_\beta e^2}{4\pi\epsilon_r\epsilon_0 r} + A_{\alpha\beta} \exp\{-B_{\alpha\beta}(r - \sigma_{\alpha\beta})\} \quad (35)$$

where e is the elementary charge and ϵ_r and ϵ_0 are the reduced dielectric constant (which we set to $\epsilon_r = 80$ for water at room temperature) and the vacuum dielectric constant, respectively. The parameter $\sigma_{\alpha\beta}$ is the distance between two ions at contact, $\sigma_{\alpha\beta} = R_\alpha + R_\beta$, where R_α is the radius of an ion of type α . In the following, we use $R_m = 20 \text{ \AA}$ and $R_i = R_c = 1 \text{ \AA}$. The exponential in Eq. (35) is an approximation to a hard sphere interaction for two ions at contact. For the parameters $A_{\alpha\beta}$ we choose $A_{mm} = 1.84 \text{ eV}$, $A_{mi} = A_{mc} = 0.0556544 \text{ eV}$, and $A_{ii} = A_{ic} = A_{cc} = 0.0051 \text{ eV}$. The parameters $B_{\alpha\beta}$ are all set to 4.0 \AA^{-1} .

We have done simulations for two different systems: The first system is a mixture of a macroion of charge $Z_m = 121$ with 471 counterions and 350 coions. The second system contains a macroion of charge $Z_m = 255$, 555 counterions, and 300 coions. In both cases, the ions are placed in a cubic simulation box of linear size $L = 160 \text{ \AA}$ using periodic boundary conditions. All the simulations are done at $T = 297 \text{ K}$. The Debye screening length λ_D is for both systems around 7.5 \AA . For the masses of the macroion and the small ions we have chosen 60 atomic units and 4 atomic units, respectively. Thus, the mass of the macroion is a factor 15 times the mass of a small ion. The Coulomb part of the potential and the forces was evaluated by means of Ewald sums with a constant $\alpha = 0.05$ and by using for the Fourier part of the Ewald sum all k vectors of magnitude less than $k_c = 2\pi\sqrt{66}/L^{29,40}$.

For the LB fluid to which the ions are coupled we use a cubic lattice with 40^3 lattice nodes. Hence, since the size of the simulation box is $L = 160 \text{ \AA}$, the lattice constant of the LB fluid is $a = 4.0 \text{ \AA}$. The counterions and coions are treated as point particles with respect to the LB fluid, i.e., each counterion and coion are equivalent to a single boundary point on the surface of the colloid. The force on each of the ions is calculated by Eq. (15). The value of the applied random force on the ion is calculated according to Eq. (22) and is equal to the random force acting on a single boundary node. The macroion is seen by the LB fluid as a sphere of radius $R_{m,LB} = 2.5a$ using the model with 66 boundary points and $\xi_0 = 6.6m_0/\tau$. The choice $R_{m,LB} < R_m$ is important if systems with more than one macroion are simulated. In this case the smaller $R_{m,LB}$ prevents that two macroions get in close contact with respect to the LB fluid.

The equations of motion were integrated with a time step of 1 fs. This very small time step is necessary because we consider explicitly counterions and coions as *microscopic* particles. A larger time step could be used if the exponential term in the potential, Eq. (35), is replaced by a softer repulsive potential. Moreover, for the update of the LB fields one could use a larger time step as for the MD part as it was done in Refs.^{16,24}. However, such optimizations were not necessary for the problems that are considered in the next section.

2. A colloidal particle in an electric field

The two systems with $Z_m = 121$ and $Z_m = 255$ are now studied in a constant electric field. This leads to a drift velocity v_d of the macroion in the direction of the field (in the following we apply a field E_x in x direction). In the linear response regime, v_d is linearly related to E_x , $v_d = \mu E_x$, where μ is the so-called electrophoretic mobility¹. The latter quantity is of particular interest because, the experimental determination of μ allows to extract the effective charge of the macroion^{41,42,43}. In the following, we determine v_d as a function of E_x and we estimate the effective charge of the macroion Z_m^* from the number of counterions that move with the macroion when the electric field is switched on.

We first equilibrated our system for 25000 time steps without the electric field and without coupling the system to the LB fluid. Fig. 9 is an equilibrium snapshot of the system with macroion charge $Z_m = 255$. One can clearly identify a spherical region around the macroion (big sphere), the so-called Debye layer, that contains an excess of counterions (small light

gray spheres) whereas the coions (small black spheres) are almost excluded from this region. Far away from the Debye layer the small ions are randomly distributed. The presence of the Debye layer can be also inferred from the radial density distributions ρ_c of counterions and coions around the macroion which are shown in Fig. 10 for the two systems with different macroion charges. In the inset of Fig. 10 the instantaneous temperature of the small ions is shown during a simulation of 10000 time step. We see that it fluctuates correctly around the assigned value for the temperature, $T = 297$ K.

After the equilibration, the system was coupled to the LB fluid and the electric field E_x was switched on. We did runs for several values of E_x ranging from $E_x = 0.0025$ V/Å to $E_x = 0.02$ V/Å. For each value of the electric field, runs over 300000 to 500000 steps were done. After reaching the steady state within about 10000 time steps, positions and velocities of the ions were stored every 500 steps to obtain the averaged quantities that are presented in the following.

Due to the electric field E_x the macroion and the coions move in the positive x direction whereas the counterions experience a force in the opposite direction. This leads to a distortion of the Debye layer which gives rise to a force opposing the motion of the macroion. This retarding force coupled with the viscous drag due to the fluid balances the force on the macroion due to E_x in the steady state. Fig. 11 shows steady state configurations of the ions for the system with macroion charge $Z_m = 255$ for two different choices of E_x , namely for $E_x = 0.01$ V/Å (top) and $E_x = 0.02$ V/Å (bottom), where the positive x direction is marked by a black arrow. It can be seen from the picture that there are more counterions behind the macroion than in front of it leading to the distorted counterion charge distribution. A high value of the electric field (Fig. 11 bottom) strips off the counterions from the shell moving along with the macroion and hence the counterion cloud becomes more diffuse.

In order to obtain an estimate of the effective charge of the macroion, we determine the average number of counterions N_c^* that move along with the macroion, i.e. those counterions are counted that have a positive drift velocity in x direction. In the limit of small electric field E_x , i.e. in the linear response regime, $|Z_i|N_c^*$ (here $Z_i = -1$) is a measure of the effective charge Z_m^* of the macroion. Hence, the ratio N_c^*/Z_m approaches one towards vanishing values of E_x if Z_m^* is equal to Z_m . Fig. 12 shows N_c^*/Z_m as a function of E_x for the two different systems with $Z_m = 121$ and $Z_m = 255$. In both cases, the linear response regime is obviously not approached, even for small considered values of E_x . However, an extrapolation

of the two curves in Fig. 12 to zero electric fields yields values close to one and thus, we can conclude from the data that Z_m^* is close to the bare charge Z_m for the systems under consideration. We also see in Fig. 12 that the slope for small E_x is smaller for the system with $Z_m = 255$ than for the one with $Z_m = 121$. This finding shows that, the smaller Z_m is, the smaller electric fields are required to obtain a reasonable estimate of the effective charge Z_m^* . That the linear response regime is not reached for our smallest considered values of E_x , is illustrated in the inset of Fig. 12 which shows the drift velocity v_d as a function of E_x . The reason that we did not do simulations for lower values of E_x is that the drift velocity approaches the order of the thermal velocity then and thus, it is difficult to yield a reasonable statistics.

The finding $Z_m^* \approx Z_m$ is in agreement with recent MD simulations^{43,44,45} of similar systems where the effective charge Z_m^* was estimated from the potential of mean force between the macroions.

VI. CONCLUSIONS

We have presented a hybrid MD/LB method for the simulation of colloidal systems that has been applied to several simple colloidal systems. Our method can be seen as an alternative to Ladd's coupling scheme^{12,13} as well as to the one proposed by Lobaskin *et al.*^{16,24} We think that all these methods (including ours) have their advantages and disadvantages and it depends on the problem whether one might prefer one or the other method.

We have applied our method to the simulation of charged colloidal systems where, apart from macroions, counterions and coions are considered in the framework of the primitive model. For such systems, our simulation technique has been used to get insight into the properties of colloids in an external electric field. This is of particular interest for the understanding of experimental studies where one extracts effective charges of macroions from the measured electrophoretic mobility^{41,42,43}. A more extensive study on this issue is in preparation.

The model with the explicit consideration of small ions has also a drawback which was already pointed out in Ref.²⁴: Only relatively small size ratios between macroions and small ions are accessible. Furthermore, only relatively small systems can be simulated due to the

long-ranged character of the electrostatic interactions. Thus, one loses partly the advantage of the LB method that mesoscopic length and time scales can be covered. However, as we have mentioned above, the DH potential describes the effective interactions between macroions surprisingly well. Therefore, we plan to study systems of, say, 1000 macroions which interact with each other via an effective DH potential. This allows then the investigation how the long-time diffusion of systems of charged colloidal particles at intermediate densities is affected by hydrodynamic interactions.

Acknowledgments: We thank Burkhard Dünweg, Vladimir Lobaskin, and Thomas Palberg for stimulating discussions. Moreover, we thank Norio Kikuchi for a critical reading of the manuscript and Hans Knoth for his help in the preparation of Figs. 9 and 11. We acknowledge financial support by the Deutsche Forschungsgemeinschaft (DFG) under Grants No. HO 2231/1 and HO 2231/2, by the SFB 625 “Von einzelnen Molekülen zu nanoskopisch strukturierten Materialien”, and by the SFB TR6 “Colloidal Dispersions in External Fields”.

* Electronic address: horbach@uni-mainz.de

- ¹ W.B. Russel, D.A. Saville, and W.R. Schowalter, *Colloidal Dispersions* (Cambridge University Press, Cambridge, 1989).
- ² There are excellent reviews on colloidal systems, e.g., P.N. Pusey, in: *Liquids Freezing and Glass Transition: II, Les Houches Sessions 1989*, eds. J.-P. Hansen, D. Levesque, and J. Zinn-Justin (North-Holland, Amsterdam, 1991), pp. 763; G. Nägele, *Phys. Rep.* **272**, 215 (1996).
- ³ R. D. Groot and P. B. Warren, *J. Chem. Phys.* **107**, 4423 (1997).
- ⁴ P. Espanol and M. Serrano, *Phys. Rev. E* **59**, 6340 (1999).
- ⁵ C.P. Lowe, *Europhys. Lett.* **47**, 145 (1999).
- ⁶ I. Pagonabarraga and D. Frenkel, *J. Chem. Phys.* **115**, 5015 (2001).
- ⁷ A. Malevanets and R. Kapral, *J. Chem. Phys.* **110**, 8605 (1999).
- ⁸ A. Lamura, G. Gompper, T. Ihle, and D. M. Kroll, *Europhys. Lett.* **56**, 319 (2001).
- ⁹ M. Ripoll, K. Mussawisade, R. G. Winkler, and G. Gompper, *Europhys. Lett.* **68**, 106 (2004).
- ¹⁰ N. Kikuchi, A. Gent, and J.M. Yeomans, *Eur. Phys. J. E* **9**, 63 (2002).
- ¹¹ N. Kikuchi, C.M. Pooley, J.F. Ryder, and J.M. Yeomans, *J. Chem. Phys.* **119**, 6388 (2003).
- ¹² A.J.C. Ladd, *J. Fluid. Mech.* **271**, 285 (1994).

- ¹³ A.J.C. Ladd, *J. Fluid. Mech.* **271**, 311 (1994).
- ¹⁴ S. Succi, *The Lattice Boltzmann Equation for Fluid Dynamics and Beyond* (Oxford University Press, Oxford, 2001).
- ¹⁵ N.-Q. Nguyen and A. J. C. Ladd, *Phys. Rev. E* **66**, 046708 (2002).
- ¹⁶ V. Lobaskin and B. Dünweg, *New J. Phys.* **6**, 54 (2004).
- ¹⁷ W. Kalthoff, S. Schwarzer, G. Ristow, and H.J. Herrmann, *Int. J. Mod. Phys. C* **7**, 543 (1996).
- ¹⁸ P. Ahlrichs and B. Dünweg, *J. Chem. Phys.* **111**, 8225 (1999).
- ¹⁹ P. Ahlrichs, R. Everaers, and B. Dünweg, *Phys. Rev. E* **64**, 040501 (2001).
- ²⁰ J. Horbach and D. Frenkel, *Phys. Rev. E* **64**, 061507 (2001).
- ²¹ F. Capuani, I. Pagonabarraga, and D. Frenkel, *J. Chem. Phys.* **121**, 973 (2004).
- ²² H. Kodama, K. Takeshita, T. Araki, and H. Tanaka, *J. Phys.: Condens. Matter* **16**, L115 (2004).
- ²³ K. Kim and R. Yamamoto, preprint cond-mat/0403350 (2004).
- ²⁴ V. Lobaskin, B. Dünweg, and C. Holm, *J. Phys.: Condens. Matter* **16**, S4063 (2004).
- ²⁵ P. Ahlrichs and B. Dünweg, *Int. J. Mod. Phys. C* **9**, 1429 (1998).
- ²⁶ A.J.C. Ladd, *Phys. Rev. Lett.* **70**, 1339 (1993).
- ²⁷ L.D. Landau and E.M. Lifshitz, *Fluid Mechanics* (Addison–Wesley, Reading, 1959).
- ²⁸ K. Heun, *Z. Math. Phys.* **45**, 23 (1900).
- ²⁹ D. Frenkel and B. Smit, *Understanding Molecular Simulation* (Academic Press, San Diego, 1996).
- ³⁰ B. Dünweg and W. Paul, *Int. J. Mod. Phys. C* **2**, 817 (1991).
- ³¹ A. Greiner, W. Strittmatter, and J. Honerkamp, *J. Stat. Phys.* **51**, 95 (1988).
- ³² W. Paul and D.Y. Yoon, *Phys. Rev. E* **52**, 2076 (1995).
- ³³ G.K. Batchelor, *An Introduction to Fluid Dynamics* (Cambridge University Press, Cambridge, 1992).
- ³⁴ H. Hasimoto, *J. Fluid Mech.* **5**, 317, 1959.
- ³⁵ A. Chatterji and J. Horbach, in preparation.
- ³⁶ B. Alder and T. Wainwright, *Phys. Rev. A* **1**, 18 (1970).
- ³⁷ M.H. Ernst, E.H. Hauge, and J.M.J. van Leeuwen, *Phys. Rev. Lett.* **25**, 1254 (1970).
- ³⁸ B. Cichocki and B.U. Felderhof, *Phys. Rev. E* **51**, 5549 (1995).
- ³⁹ B. Cichocki and B.U. Felderhof, *Phys. Rev. E* **62**, 5383 (2000).
- ⁴⁰ M.P. Allen and D.J. Tildesley, *Computer Simulation of Liquids*, (Clarendon), Oxford, 1987.

- ⁴¹ D. Hessinger, M. Evers, and T. Palberg, *Phys. Rev. E* **61**, 5493 (2000).
- ⁴² P. Wette, H. J. Schöpe, and T. Palberg, *J. Chem. Phys.* **116**, 10981 (2002).
- ⁴³ L. Shapran, M. Medebach, P. Wette, T. Palberg, H.J. Schöpe, J. Horbach, T. Kreer, and A. Chatterji, *Coll. Surf. A*, accepted for publication (2005).
- ⁴⁴ T. Kreer, J. Horbach, A. Chatterji, submitted to *Phys. Rev. E* (2005).
- ⁴⁵ E. Allahyarov, H. Löwen, and S. Trigger, *Phys. Rev. E* **57**, 5818 (1998).

VII. LIST OF CAPTIONS

Fig. 1: Sketch of the model for a colloidal particle. The centres of the small spheres represent the points at which the colloidal particle interacts with the LB fluid. The cylinders that connect the spheres with each other are just guides to the eye.

Fig. 2: $1/\xi_L$ for particle of radius $R = 2.5a$ as a function of $1/L$ for the indicated values of ξ_0 . The dashed lines are fits with Eq. (33) and the solid lines is a fit with Eq. (32) for $\xi_0 = 19.8m_0/\tau$ using the hydrodynamic radius R_h as a fit parameter. The inset shows the variation of the hydrodynamic radius R_h normalized by the assigned sphere radius R as a function of ξ_0 (see text).

Fig. 3: ξ_L as a function of the particle radius R for $\xi_0 = 13.2m_0/\tau$ and the system sizes $L = 60a$ and $L = 80a$.

Fig. 4: Time-dependent velocity correlation function $C_v(t)$ (solid lines) of the colloidal particle and normalized average velocity $v_s(t)/V(0)$ of the LB fluid at the surface of the particle (dashed lines) for a) $\xi_0 = 0.66 m_0/\tau$, b) $\xi_0 = 3.3 m_0/\tau$, c) $\xi_0 = 6.6 m_0/\tau$, and d) $\xi_0 = 13.2 m_0/\tau$. The box length was set to $L = 40a$, the radius of the particle to $R = 2.5a$, and its mass to $M = 120m_0$. The dotted lines are exponential functions $f(t) = \exp(-\frac{\xi_0}{M}t)$ that describe the short-time decay of $C_v(t)$ (note that no fit parameter is involved).

Fig. 5: $C_v(t)$ for $\xi_0 = 6.6 m_0/\tau$ at the indicated system sizes. The dotted line shows the power law $f(t) = At^{-3/2}$ (see text).

Fig. 6: The same as in Fig. 5 but now for the angular velocity correlation function $C_\omega(t)$ and for $\xi_0 = 13.2m_0/\tau$. The dotted line shows the power law $f(t) = Bt^{-5/2}$ (see text).

Fig. 7: Velocity autocorrelation function for $\xi_0 = 6.6m_0/\tau$ and $L = 40a$ as calculated for a kicked particle (solid line) and with thermal fluctuations (circles).

Fig. 8: The same as in Fig. 7 but now for the angular velocity correlation function.

Fig. 9: Representative configuration of counterion and coion distribution around a macroion of charge $Z_m = 255$. The macroion is the central large grey sphere, the 555 counterions are the light gray coloured small spheres and the 300 coions are the black small spheres.

Fig. 10: Plot of the radial density distribution $\rho_m(r)$ of counterions and coions around the macroion for the two indicated charges Z_m . The system with $Z_m = 255$ contains 555 counterions and 300 coions whereas there are 471 counterions and 350 coions in the system

with $Z_m = 121$. The inset shows the fluctuation of the temperature T of the counterions around its assigned value (solid line).

Fig. 11: Snapshot of the ionic distribution around the macroion (for the system with $Z_m = 255$) with an applied electric field of $E_x = 0.01 \text{ V/\AA}$ (top) and $E_x = 0.02 \text{ V/\AA}$ (bottom), respectively. The electric field is applied in the direction of the black arrow. The rest is similar to Fig. 9.

Fig. 12: N_c^*/Z_m as a function of the external electric field E_x . N_c^* is the average number of counterions that move with the particle. The inset shows the drift velocity v_d as a function of the electric field E_x .

VIII. LIST OF FIGURES

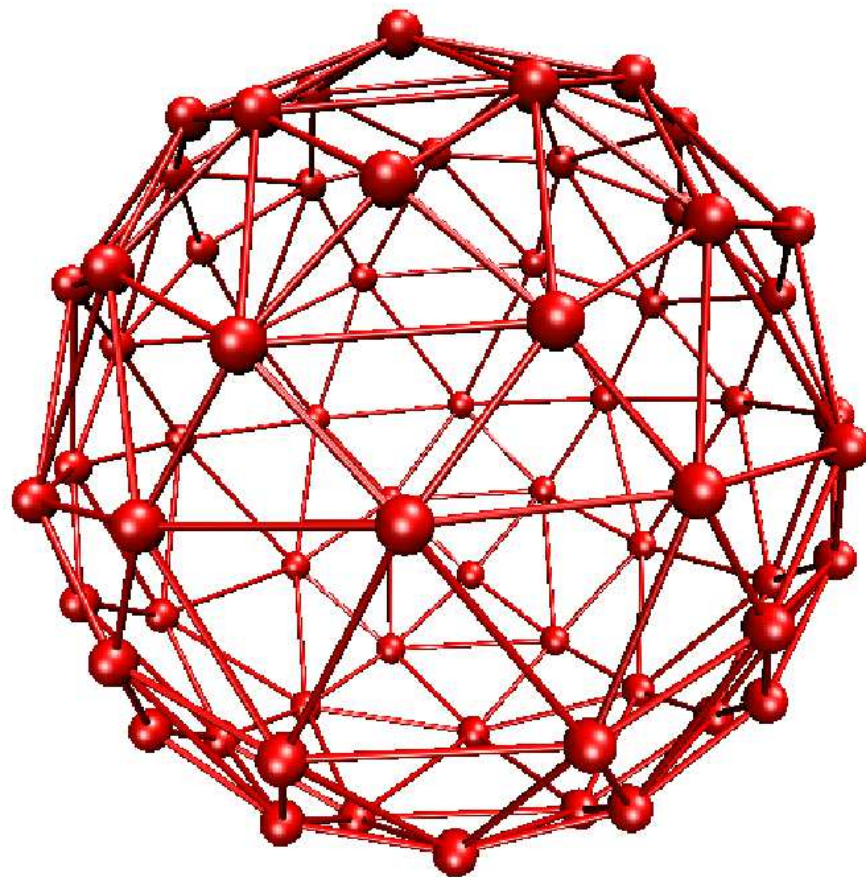


FIG. 1:

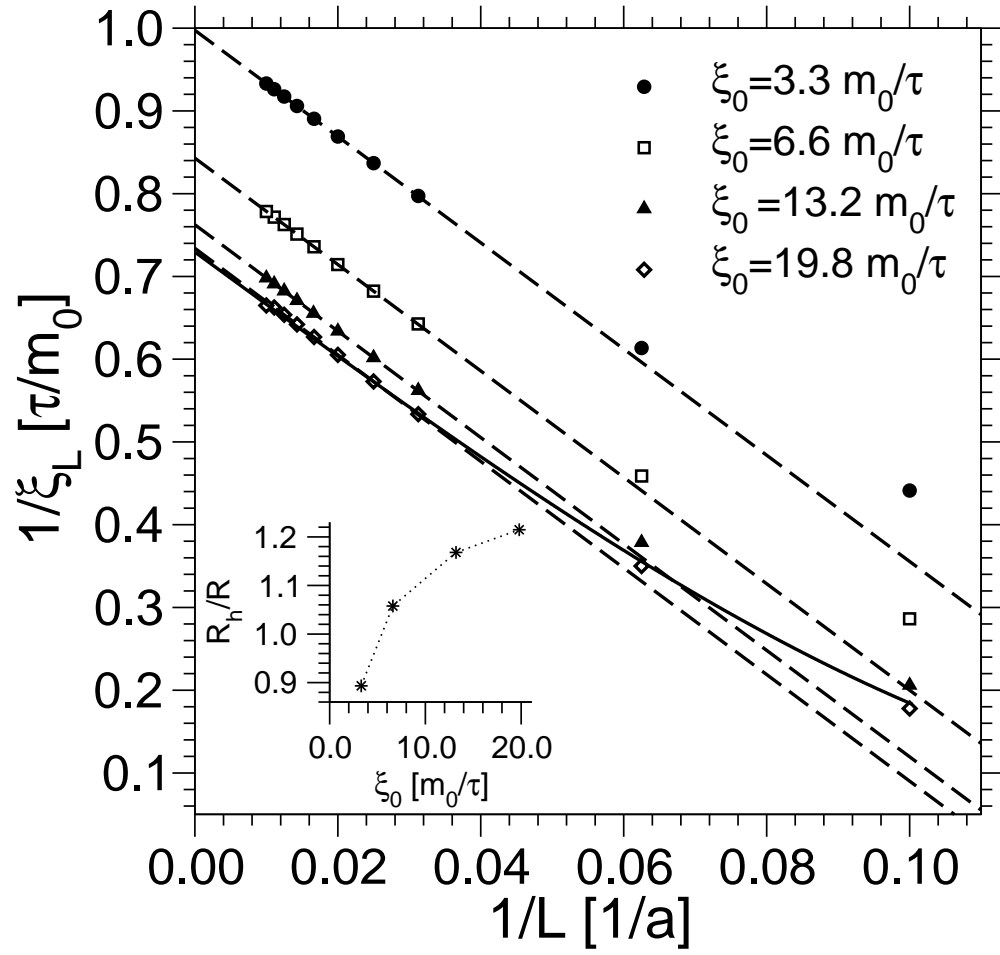


FIG. 2:

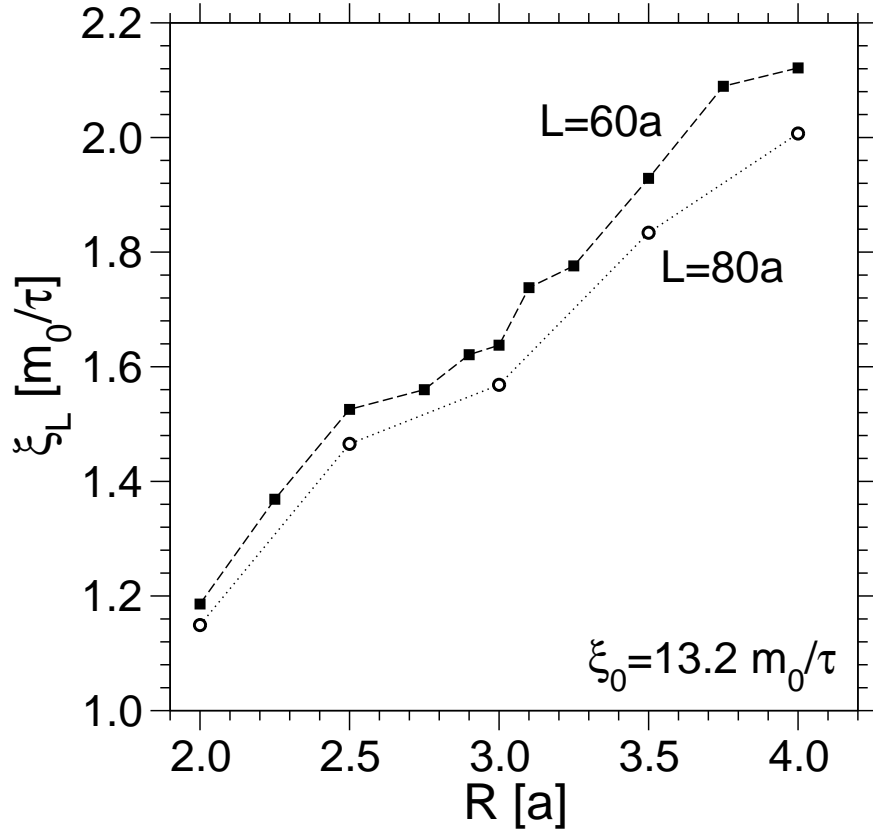


FIG. 3:

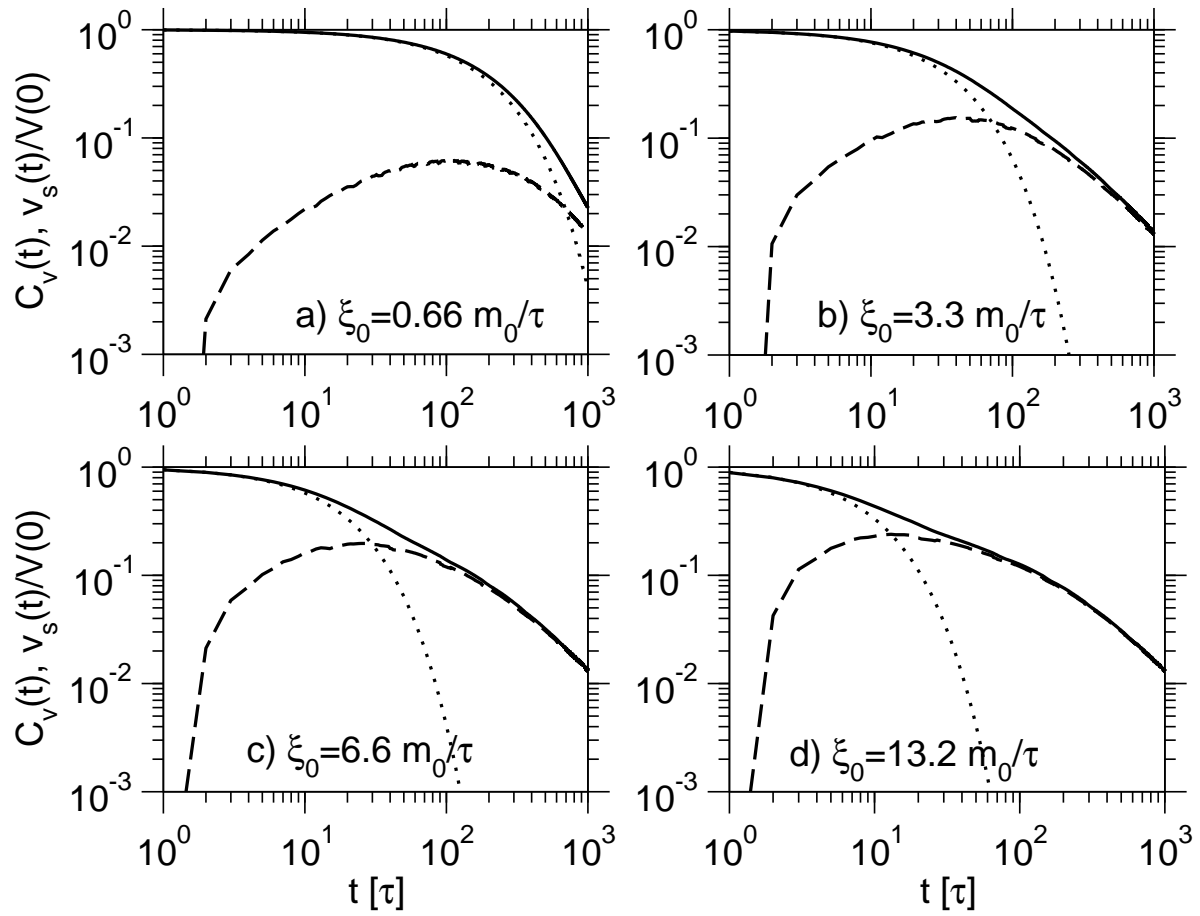


FIG. 4:

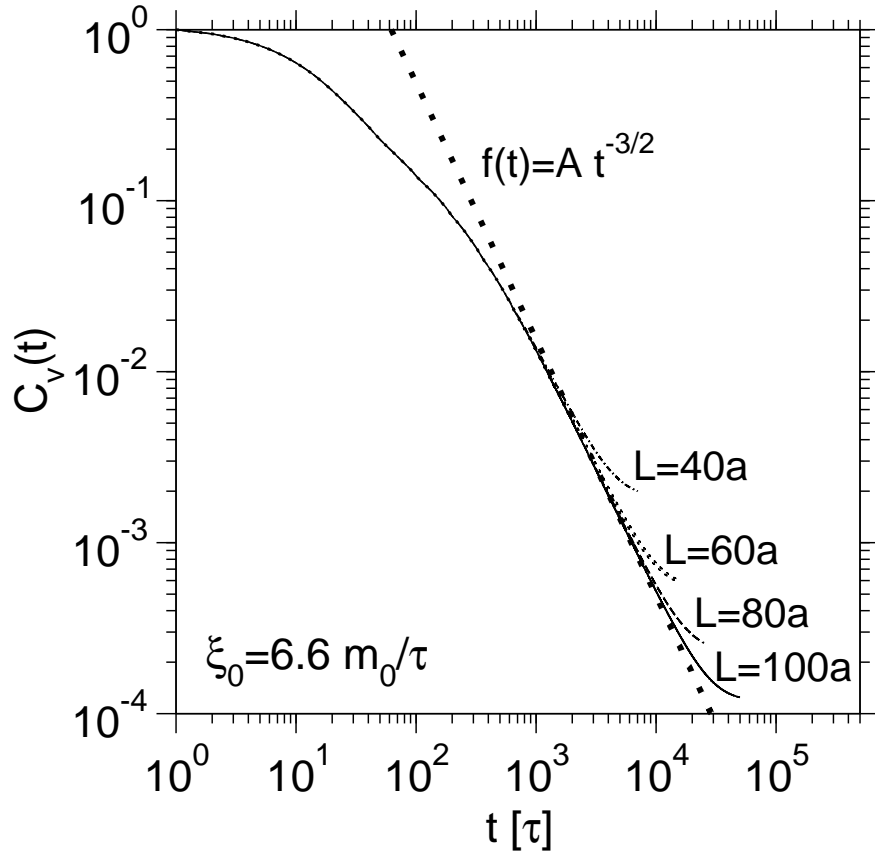


FIG. 5:

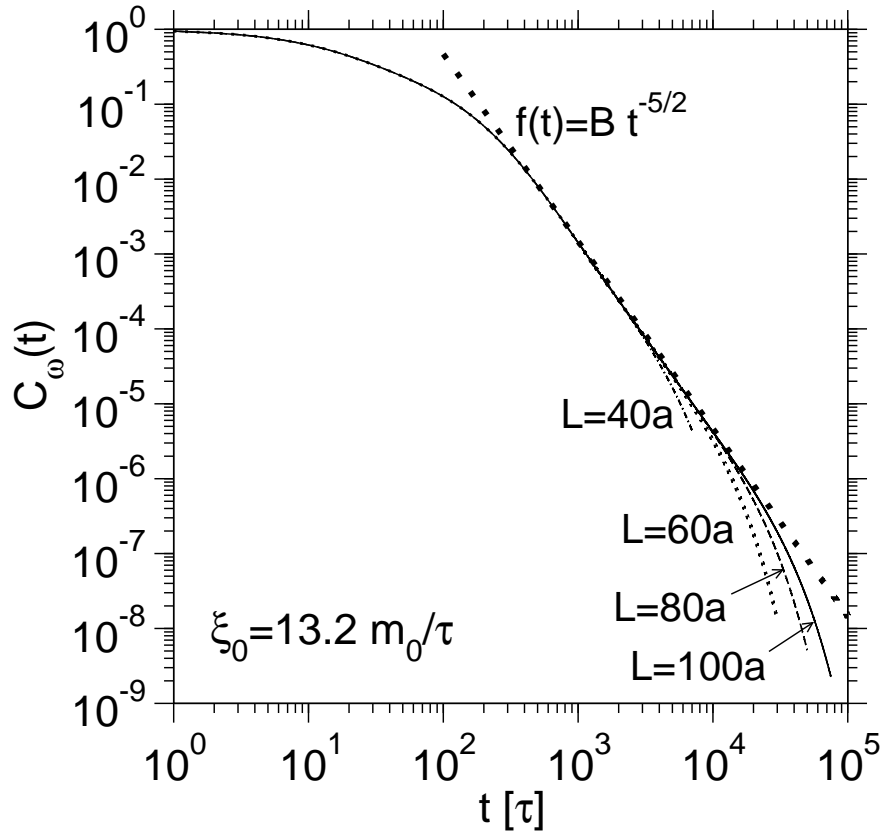


FIG. 6:

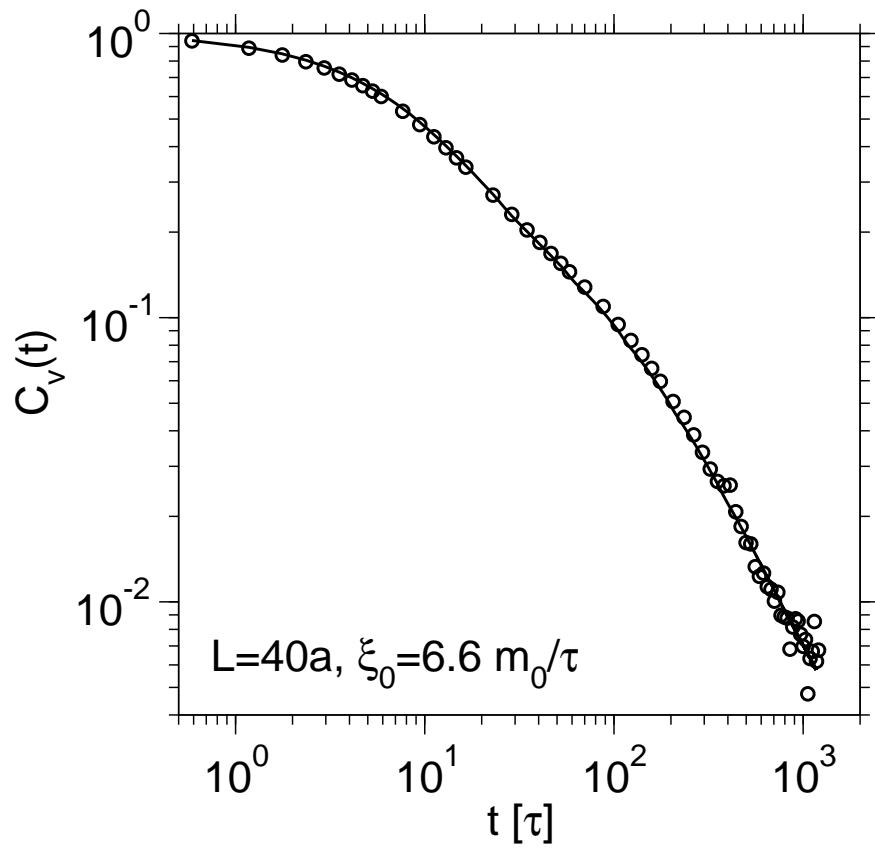


FIG. 7:

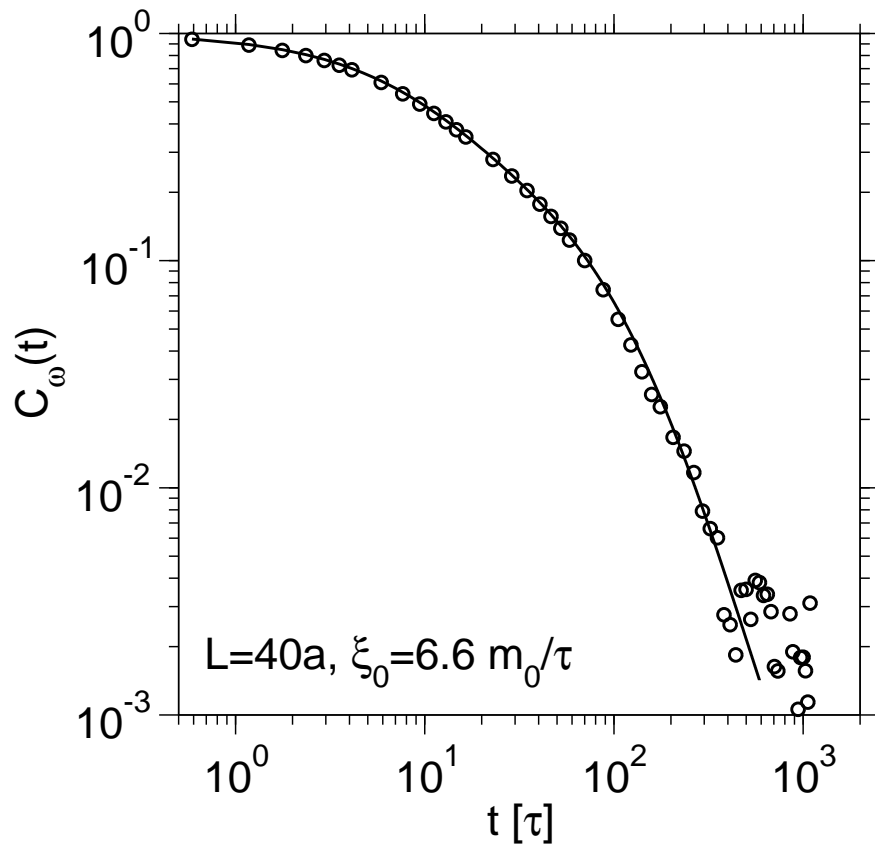


FIG. 8:

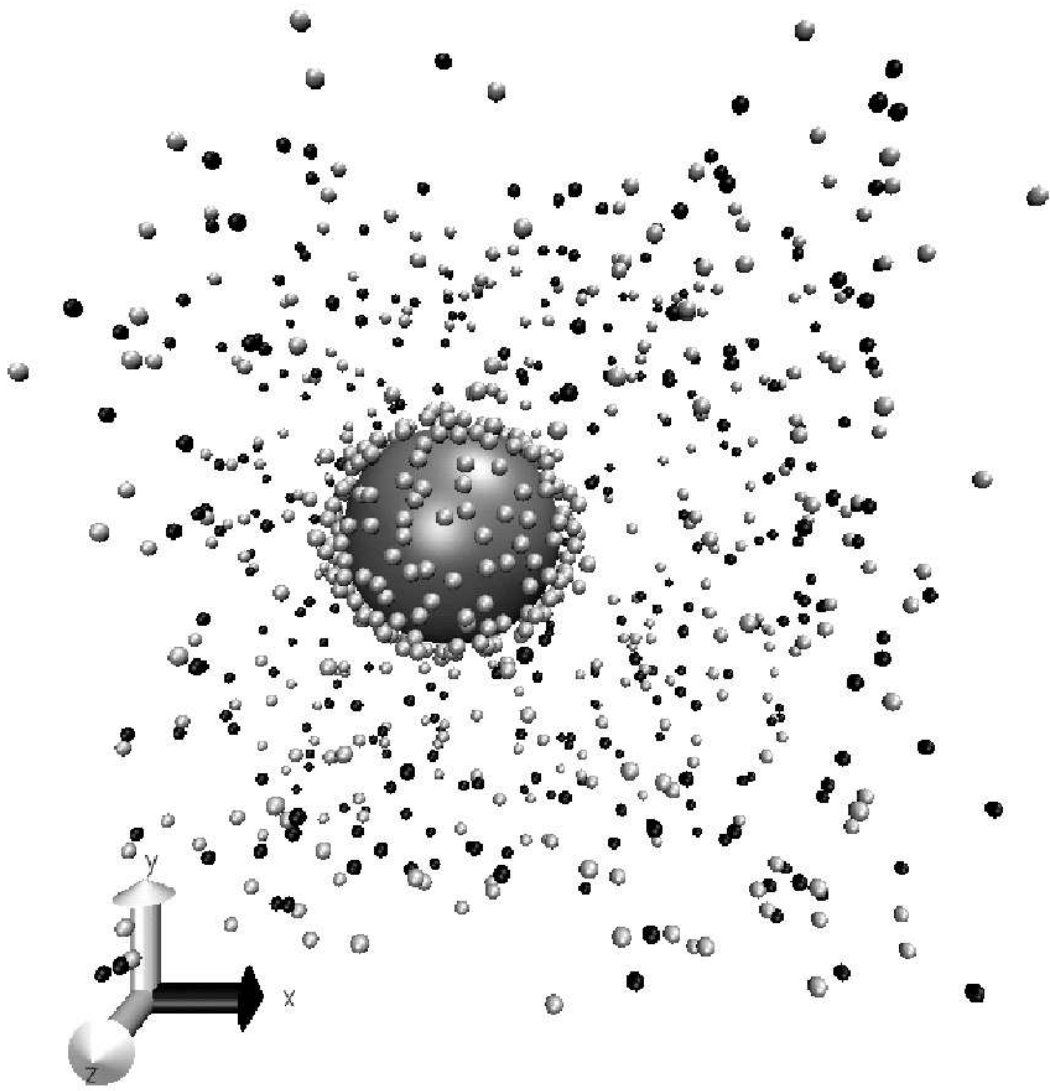


FIG. 9:

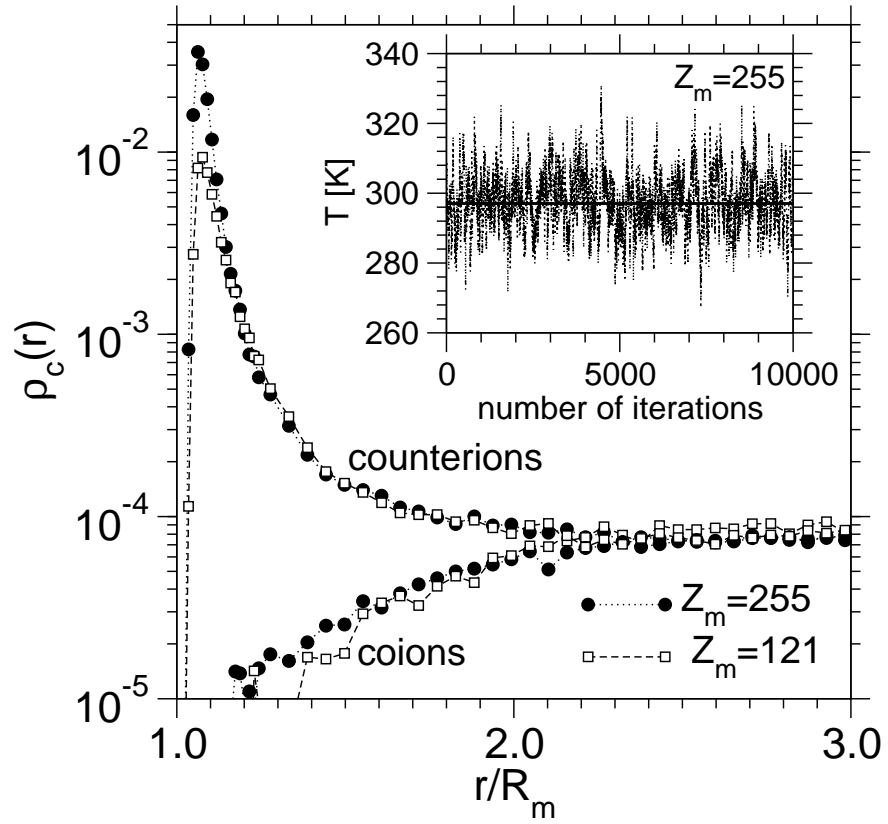


FIG. 10:

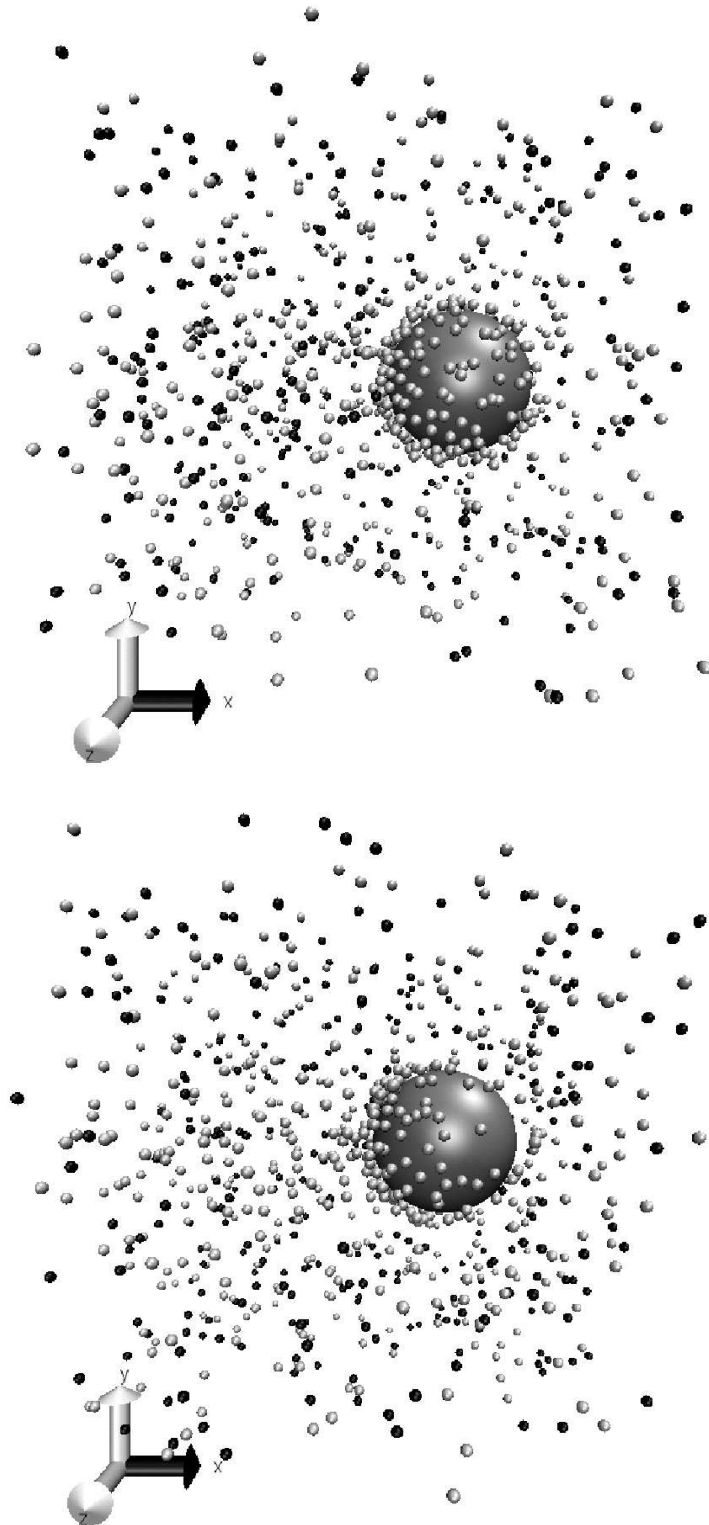


FIG. 11:

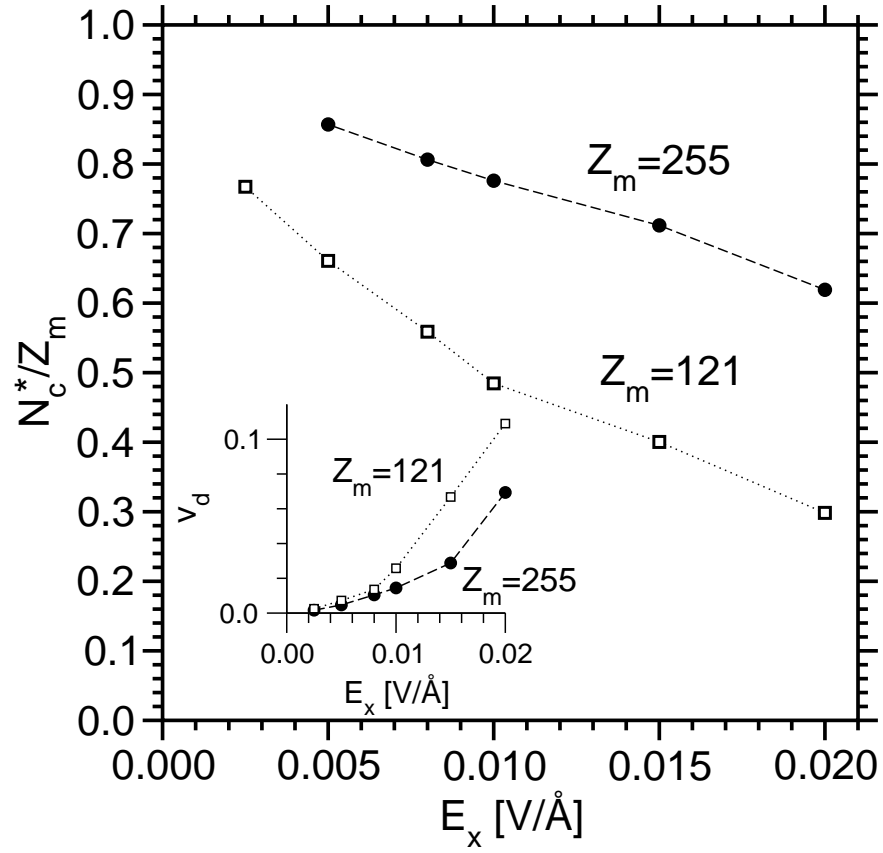


FIG. 12: